

Earth Observation and Geomatics Engineering

Homepage: https://eoge.ut.ac.ir/

Online ISSN: 2588-4360

A Hybrid Under-Cloud Gap Filling Approach for LST Estimation Using MODIS and Meteorological Station Data

Ramin Saadi Esfangareh¹ (parta) na Kalin Akhoondzadeh²™ (parta) mehrdad Eslami³ **(parta)**

- 1. School of Surveying and Geospatial Engineering, University of Tehran, Tehran, Iran. E-mail: ramin.saadi@ut.ac.ir
- 2. Corresponding author, School of Surveying and Geospatial Engineering, University of Tehran, Tehran, Iran. E-mail: makhonz@ut.ac.ir
- 3. Faculty of Payambar Azam, Imam Hossein University, Tehran, Iran. E-mail: meslami@ihu.ac.ir

Article Info

Article type: Research Article

Article history:

Received 2025-04-15 Received in revised form 2025-06-23 Accepted 2025-07-28 Published online 2025-10-19

Keywords:

Reconstruction, Cloud cover, Modis,

ABSTRACT

Land Surface Temperature (LST) is a key parameter in climate and environmental studies, influencing ecosystem processes and biological dynamics at various scales. This study aims to address the limitation of spatial coverage in ground-based LST observations and the challenge of cloud-induced data gaps in satellite thermal remote sensing.

A novel hybrid approach was developed to reconstruct LST in cloudy regions using MODIS satellite data and ground-based meteorological observations. The methodology involves training a Random Forest (RF) regression model on MODIS brightness temperature bands (31 and 32) and ground station data. For cloud-covered regions, two reconstruction scenarios were implemented: (1) interpolation-based estimation using Inverse Distance Weighting (IDW) refined by RF, and (2) index-based estimation using MODIS-derived indices such as NDVI, NDBI, and NDMI. A genetic algorithm (GA) was employed to combine the outputs of both scenarios by optimizing their weights to minimize estimation error.

The hybrid approach achieved an RMSE of 0.78°C, representing an improvement of approximately 0.8°C over the individual reconstruction scenarios. The optimized integration of RF and GA effectively enhanced the accuracy and continuity of reconstructed LST under cloudy conditions.

This study demonstrates that combining satellite data with ground-based observations through a machine learning-driven hybrid framework can effectively overcome the limitations of cloud-contaminated pixels. The proposed method provides a reliable solution for generating continuous and accurate LST maps and holds significant potential for improving thermal remote sensing applications in complex environments.

Cite this article: Saadi Esfangareh, R, Akhoondzadeh, M., & Eslami, M. (2025). A Hybrid Under-Cloud Gap Filling Approach for LST Estimation Using MODIS and Meteorological Station Data, Earth Observation and Geomatics Engineering, Volume 8, Issue 2, Pages 67-80. http://doi.org/10.22059/eoge.2025.393513.1174



© The Author(s).

DOI: http://doi.org/10.22059/eoge.2025.393513.1174

Publisher: University of Tehran.

1. Introduction

Remote Sensing (RS) has a wide range of applications, including urban planning, forest and wetland management, and global warming studies. LST plays a crucial role in both ecosystems and the Earth's atmospheric system (Mo et al., 2021; X. Yu et al., 2014; Zhou et al., 2019). LST is widely used in various applications such as urban heat island analysis, health studies, and drought monitoring (Huang et al., 2013; Liu & Weng, 2009; Mallick et al., 2013; Ullah et al., 2020). Additionally, LST serves as a key variable in ecological, meteorological, and biological models of the Earth's system.

Traditionally, LST is measured at weather stations with high temporal resolution as point-based values. However, due to the high cost and labor required for their maintenance, the number of these stations is limited (Cho et al., 2022). Remote sensing provides an effective alternative by enabling large-scale, continuous LST measurements (Mo et al., 2021). Various methods have been developed for LST retrieval, including the single-channel method (Jiménez-Muñoz & Sobrino, 2003), the Wan-Dozier split-window method (Wan & Dozier, 1996), the Jiménez-Muñoz splitwindow method (Jiménez-Muñoz et al., 2014), and the Rozenstein split-window method (Rozenstein et al., 2014). Moreover, several satellite datasets, such as MODIS (Wan, 2008), ASTER (Gillespie et al., 1998), and CGLS (Freitas et al., 2013) have been widely used as sources of Thermal Infrared (TIR) data for LST retrieval. MODIS LST, in particular, is a primary source due to its wide coverage, free access, and optimal temporal resolution (Zhao et al., 2020).

One of the key advantages of remotely sensed LST data is its global coverage. However, at a local scale, cloud cover remains a major challenge, as clouds obscure TIR signals, leading to missing LST values in affected areas (Jin & Dickinson, 1999; L. Lu et al., 2011). As a result, gap-filling techniques to estimate LST in cloud-covered regions have become a crucial area of research in remote sensing (Mo et al., 2021).

Numerous studies have proposed two main approaches for filling gaps in LST datasets caused by cloud cover (Zhao et al., 2020). The first approach estimates missing pixels based on spatial and temporal interpolation techniques, using neighboring high-quality MODIS LST data. These methods include Fourier transform, Harmonic Analysis of Time Series (HANTS), and Savitzky-Golay (S-G) filtering (Na et al., 2014; Scharlemann et al., 2008; Xu & Shen, 2013). Geostatistical interpolation methods such as spline and kriging interpolation have also been employed. Some studies have used temporal interpolation to estimate missing

LST values from the Aqua satellite (afternoon overpass) based on Terra satellite data (morning overpass) (Crosson et al., 2012). Additionally, (W. Yu et al., 2015) proposed a method using a transfer function with the most similar pixels to estimate missing values. While these approaches effectively utilize neighboring spatial or temporal information, they often fail in topographically complex areas or regions with large data gaps, where sparse data limits reliable estimation (Zhao et al., 2020).

The second approach addresses cloud-induced gaps by leveraging correlation models and auxiliary datasets. Some studies have used Digital Surface Models (DSM) to reconstruct MODIS LST values based on long-term temperature gradients, achieving reliable results in mountainous regions (Neteler, 2010). Others have employed regression models incorporating auxiliary predictors such as longitude, latitude, altitude, and NDVI to estimate missing LST values in 8-day composite datasets (Fan et al., 2014). Additional auxiliary datasets—including land cover maps, MODIS Band 7, solar radiation, slope, distance from forests and oceans—have also been utilized to enhance estimation accuracy. These auxiliary datasets provide valuable information for reconstructing missing LST values by considering terrain complexity and spatial heterogeneity (Zhao et al., 2020).

In recent years, deep learning methods have shown promising results in LST reconstruction under cloud-covered conditions. For instance, (Wu et al., 2022) introduced a method using convolutional neural networks (CNN) in combination with spatiotemporal fusion of MODIS and Landsat data to reconstruct high-resolution LST in cloudy scenes. Similarly, (Gong et al., 2023) proposed a spatiotemporal attention-based deep learning framework that effectively modeled complex spatial-temporal dependencies to estimate LST under cloudy conditions with high accuracy. Although these approaches demonstrate state-of-the-art performance, they often require large training datasets, significant computational resources, and may suffer from limited interpretability, making them less accessible for operational or region-specific applications.

while previous studies have made progress using either interpolation or regression-based gap-filling techniques, several limitations remain. Physically-based models often depend on complex energy balance equations and require numerous atmospheric and surface parameters, which may not be available or accurate under cloudy conditions (Fu et al., 2019). Deep learning approaches have also been explored; however, they typically demand extensive labeled datasets, involve high computational costs, and often function as black boxes, reducing interpretability(Kustura et al., 2025). In contrast, RF, a non-parametric ensemble

learning method, handles non-linearities and highdimensional heterogeneous data effectively with relatively low computational requirements. Its robustness, interpretability, and ability to integrate multiple data sources make it a suitable choice for this study(Wang et al., 2024). Furthermore, most existing methods do not fully leverage a hybrid strategy that integrates spatial interpolation, spectral indices, and machine learning, optimized by evolutionary algorithms. The proposed method addresses these gaps by combining the strengths of multiple approaches into a unified, flexible framework

In this study, we introduce a novel method that integrates both interpolation-based and auxiliary-data-based approaches to reconstruct under-cloud LST values using MODIS satellite imagery and ground station data. A RF model is employed to map MODIS Brightness Temperature data to ground-based temperature measurements, generating a continuous LST map for Iran. For cloud-covered regions, advanced interpolation techniques and satellite-derived indices are applied, with their outputs optimally combined using a GA.

2. Study Area

The initial step of this study involved modeling nearsurface temperatures across Iran (Figure 1). This was achieved using brightness temperatures derived from bands 31 and 32 of the MODIS satellite, alongside daily ground temperature observations collected from meteorological stations. Data from 820 meteorological stations distributed across Iran were utilized for this purpose.



Figure 1. Study Area (Iran)

Iran encompasses a diverse range of climatic zones, including arid, semi-arid, Mediterranean, subtropical, cold and mountainous, desert, and continental and steppe. The central and eastern regions are predominantly arid and

semi-arid, characterized by low annual precipitation and high temperatures, making agriculture and water resources a challenge.

The Varamin Plain, located southeast of Tehran, features an arid to semi-arid climate, characterized by low annual precipitation and considerable temperature variability. Its flat topography and fertile soils have historically supported extensive agricultural activities, making it a significant region within Tehran Province. Given these characteristics, Varamin (Figure 2) was selected as a representative case study to evaluate the performance of the proposed undercloud temperature reconstruction method.

A virtual cloud mask was created for this region, and the under-cloud temperature was then reconstructed using the proposed method. This area was chosen as a representative case to evaluate and demonstrate the performance of the proposed approach.

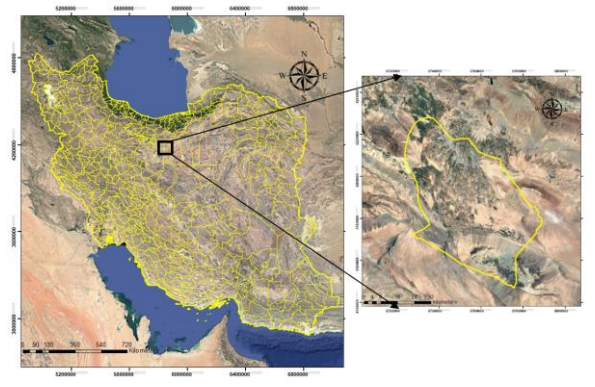


Figure 2. Cloud mask region for virtual cloud simulation (Varamin City)

3. Dataset Description

This study utilized two datasets: daily temperature data from meteorological stations and MODIS satellite imagery. A detailed explanation of each dataset is provided below.

3.1. Weather Station Data

Daily temperature data from 820 ground meteorological stations across Iran were collected for the period from 2000 to 2022. These data were considered highly reliable and were used as a reference for reconstructing LST using MODIS imagery. Figure 3 illustrates the distribution of these stations across Iran.

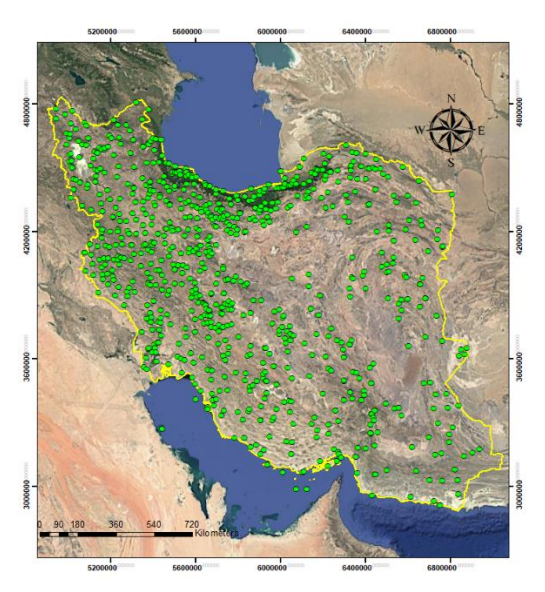


Figure 3. Distribution of Ground-based Meteorological Stations in the Study Area

3.2. Satellite Data

This study used satellite imagery from the MODIS sensor. The MODIS instrument, which is on the Terra and Aqua satellites by NASA, has a wide spectral and spatial resolution to observe the Earth. The bands and products used are detailed below:

Brightness Temperature Bands: The bands 31 (10.78–11.28 μ m) and 32 (11.77–12.27 μ m) in the thermal infrared range. These bands are well applied in order to derive surface temperature of the Earth because of their high response to thermal radiation emitted by the surface.

Products: NDVI, NDBI, NDMI, NDSI, and Land Cover (LC) products.

Spatial Resolution: The thermal bands used have a spatial resolution of 1 km. All other products were resampled to the same spatial resolution for consistency.

Temporal Resolution: MODIS imagery provides daily global coverage, making it highly suitable for calculating LST.

3.2.1. Advantages of MODIS Data for LST Calculation

High Temporal Frequency: Daily coverage allows for continuous monitoring of temperature patterns.

Spectral Sensitivity: Bands 31 and 32 are specifically designed for thermal emission, ideal for LST retrieval.

Accessibility: MODIS data is freely available at no cost.

3.2.2. Time Coverage

Three specific dates were selected to analyze varying cloud conditions and validate the proposed method:

- June 12, 2022
- June 19, 2022
- June 21, 2022

4. Methodology

This study aims to reconstruct LST under clouds using a novel hybrid approach that integrates ground-based meteorological station data, MODIS Brightness Temperature (BT) and products, advanced interpolation techniques, and machine learning models. The methodology is detailed in the following sections and is illustrated in the accompanying flowcharts (Figures 4, 5, and 6).

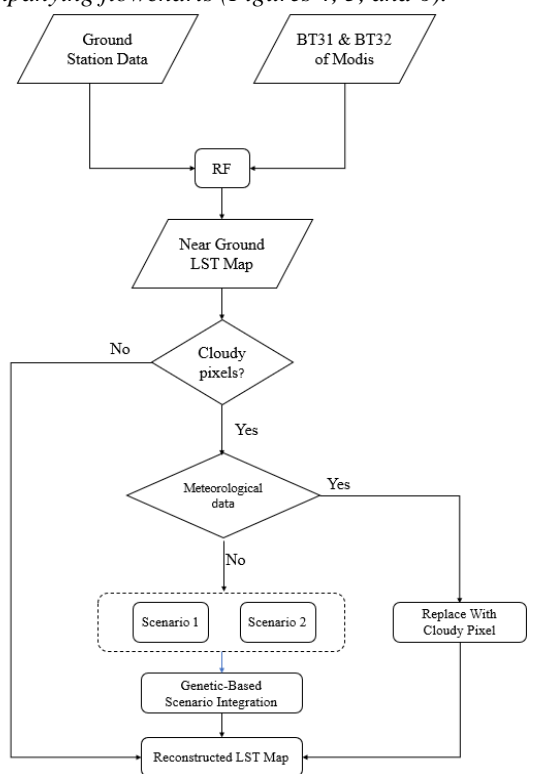


Figure 4. Overall Workflow for LST Reconstruction in Cloud-Covered Regions

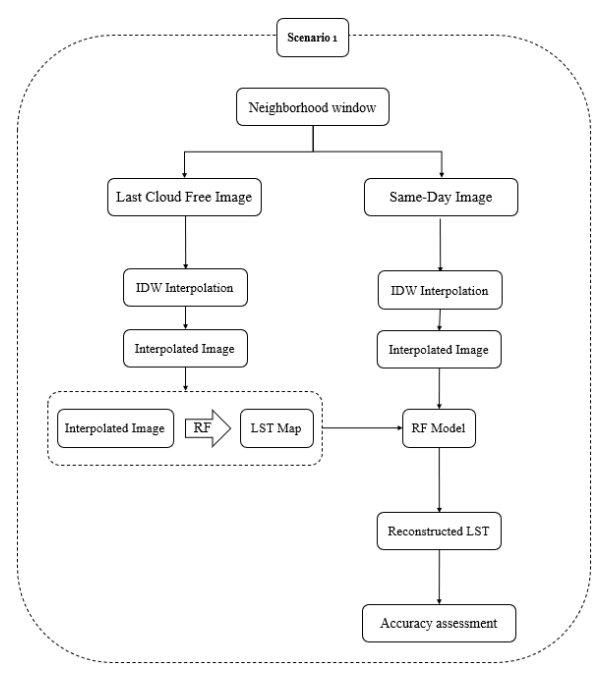


Figure 5. Scenario 1: Interpolation based LST Reconstruction

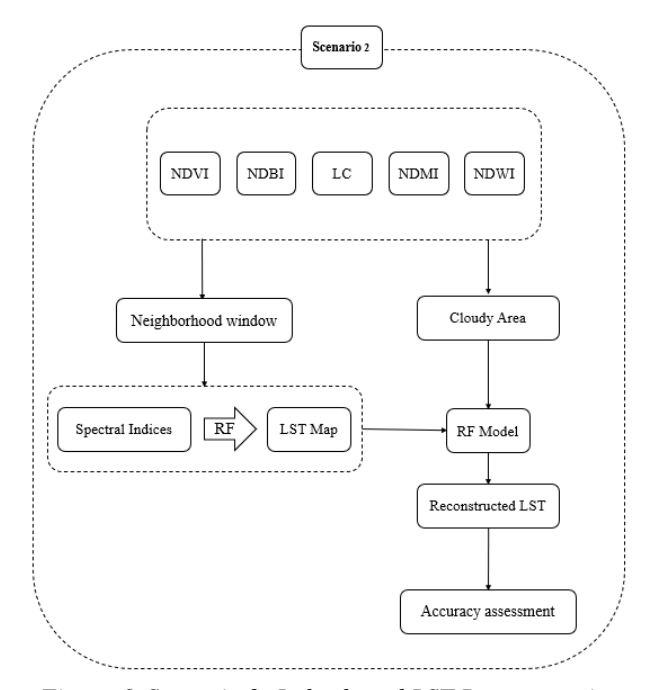


Figure 6. Scenario 2: Index based LST Reconstruction

The overall flowchart of this study, illustrating the framework and main processes, is presented in Figure 4.

This framework encompasses data collection and LST reconstruction under two different scenarios. Detailed explanations of each scenario are provided separately in Figures 5 and 6.

4.1. Data Collection and Preprocessing

4.1.1. Ground-Based Data Collection

In this study, daily near-surface temperature data from 820 meteorological stations across Iran were utilized, covering the period from 2000 to 2022. These stations provided point-based temperature observations with high temporal resolution. For each station, the corresponding pixel was extracted from the MODIS brightness temperature (BT) data—specifically from bands 31 and 32—on cloud-free days. These ground observations were later used both for training the RF model and for evaluating the accuracy of reconstructed LST in cloud-covered areas.

4.1.2. Satellite Data Preprocessing

To ensure the quality and consistency of the satellite data used in the reconstruction framework, several preprocessing steps were applied. MODIS LST products (MOD11A1) and MODIS surface reflectance products (MOD09GA) were used as the primary satellite inputs.

Only clear-sky pixels were retained based on MODIS quality assurance (QA) flags. Pixels identified as cloudy, low-quality, or with uncertain retrieval conditions were excluded. All reflectance products used for calculating indices (e.g., NDVI, NDBI, NDMI, NDSI) are atmospherically corrected using standard MODIS algorithms.

Spatially, all satellite layers were resampled to a consistent 1 km resolution, reprojected to the WGS84 coordinate system, and cropped to the extent of the study area. Furthermore, all satellite inputs were temporally aligned to ensure consistency in model reconstruction and evaluation. These steps were essential to improve data reliability, reduce noise, and enable accurate LST modeling.

4.2. Random Forest

RF regression is a machine learning technique that combines an ensemble of regression trees on the principles of ensemble learning(Breiman, 2001). The model is based on the "random association of trees" algorithm, an ensemble technique of decision trees. It is a highly suitable technique for high-dimensional data with a large number of features and suits both classification and regression tasks.

In this approach, each tree independently predicts a subset of the training data, and the predictions are combined. The algorithm ensembles a set of independent decision trees, where each tree randomly samples the data and organizes it hierarchically to make a prediction. By fitting each tree to a different subset of the data, the algorithm gains model diversity and makes overfitting less likely. The final prediction is then made by integrating the output of all the trees, giving a better and more credible result.

4.3. Cloud Analysis and Temperature Reconstruction

Each pixel in the MODIS imagery was examined to determine whether it was cloud-covered. For cloud-free pixels, the modelled ground-level temperatures were retained. For cloud-covered pixels, the methodology included two scenarios depending on the availability of ground station data for the corresponding pixel location:

- If ground station data were available: The measured ground temperature from the station was directly substituted for the cloud-covered pixel.
- If ground station data were unavailable: Two alternative reconstruction scenarios were implemented to estimate under-cloud temperatures.

4.4. Scenario 1: Interpolation with Enhanced Accuracy

In this scenario, the cloud-covered area was analysed using a spatial neighborhood window:

- An initial estimation of under-cloud temperatures was performed using Inverse Distance Weighting (IDW) interpolation, based on the surrounding cloud-free pixels.
- 2. To improve accuracy, the same interpolation process was applied to the corresponding neighborhood in the MODIS image from the most recent cloud-free day.
- 3. A RF regression model was developed to establish a relationship between the interpolated values and the actual ground temperatures on the cloud-free day. This model was then applied to the interpolated temperatures on the cloudy day, refining the undercloud temperature estimates.

4.4.1. Inverse Distance Weighting (IDW)

IDW is an interpolation method used to estimate the value of an unknown point in space based on the values of surrounding known points. In this approach, the contribution of each known point is weighted inversely proportional to its distance from the target point. Closer points have a greater influence on the estimation, while farther points contribute less. This makes IDW effective for spatial data analysis where proximity is a key factor(G. Y. Lu & Wong, 2008).

$$Z = \frac{\sum_{i=1}^{n} (\frac{Z_i}{d_i})}{\sum_{i=1}^{n} (\frac{1}{d_i})}$$
(1)

4.5. Scenario 2: Index-Based Modelling

For this scenario, MODIS-derived indices NDVI, NDBI, NDMI, and NDWI, along with land cover classification information, were extracted from the MODIS products for the most recent cloud-free day. On the cloudy day, the spatial neighborhood of the cloud-covered region was defined, and a RF regression model was developed using the indices on the cloud-free day as predictors and ground temperatures as the response variable. Since the index values were already calculated for the cloud-covered region, this model was employed to reconstruct the undercloud temperatures on the cloudy day.

4.6. Hybrid Model Integration Using GA

To improve the accuracy of under-cloud LST reconstruction, the outputs of Scenario 1 (interpolation-based) and Scenario 2 (index-based) were combined using a GA. The goal was to determine an optimal set of weights $(w_1 \text{ and } w_2)$ assigned to each scenario's LST output in a weighted linear combination, such that:

$$LST_{Combined} = w_1 * LST_{S1} + w_2 * LST_{S2},$$

$$subject\ to\ w_1 + w_2 = 1$$
 (2)

The optimization objective was to minimize the RMSE between the combined LST and ground-truth LST values within the virtual cloud mask area. The RMSE served as the fitness function for the GA. The algorithm iteratively evolved candidate weight pairs over 100 generations using standard crossover and mutation operations to find the weight configuration that minimized error.

This integration enabled the method to benefit from the local accuracy of interpolation (Scenario 1) and the generalization capability of spectral indices across heterogeneous landscapes (Scenario 2). Table 5 presents the final weights derived from the GA, while Table 6 demonstrates the improved performance of the integrated approach.

4.7. Model Evaluation

The performance of the proposed methodology was evaluated using standard statistical metrics, including Root

Mean Square Error (RMSE), correlation coefficient (R), and the coefficient of determination (R²). These metrics were used to compare the reconstructed under-cloud temperatures with the LST map created from the initial model using ground station data and MODIS BT values. By using RMSE, R, and R², the evaluation provided a comprehensive understanding of the model's effectiveness in estimating accurate under-cloud temperatures.

4.8. Optimization of Scenario Weights Using GA
To optimally combine the outputs from Scenario 1 and
Scenario 2, a GA was employed. The objective was to
determine the best weighting scheme for the two LST
reconstruction methods, such that the Root Mean Square
Error (RMSE) between the combined image and actual
ground-truth LST is minimized. The GA was implemented
with the settings listed in Table 1.

Table 1. Hyperparameters of the GA

Parameter	Value	Description
Population size	100	Number of solutions in each generation
Number of generations	100	Number of evolutionary cycles
Lower bounds (lb)	[0, 0]	Minimum allowed weights for each scenario
Upper bounds (ub)	[1, 1]	Maximum allowed weights for each scenario
Number of variables	2	Two weights (Scenario 1 and Scenario 2)
Fitness function	RMSE	Based on difference between predicted and actual LST
Crossover function	Default (2- point)	Combines weights from parent solutions
Mutation rate	Automatic	default adaptive mutation
Random seed	6	To ensure reproducibility

5.Result and Discussion

This section analyzes the temperature reconstruction results for the under-cloud region in two scenarios. Table 1 summarizes the evaluation results for each scenario and the combined method using various validation criteria.

5.1. RF Model for LST Prediction

In the first step, a RF model was developed using data from meteorological ground stations and the brightness temperatures of MODIS bands 31 and 32. Once the model was built, the LST for the entire country of Iran was generated. The resulting LST map is shown in Figure 7, which provides a continuous prediction of the near-surface temperature across Iran. The model's performance was assessed using RMSE, R, and R² criteria. The evaluation results are presented in Table 2.

Table 2. Model Evaluation Metrics for LST Prediction

	$RMSE(C^{\bullet})$	R	R^2
BT31	4.69	0.88	0.78
BT32	2.75	0.96	0.92
BT31&BT32	2.39	0.97	0.93

The output map of the LST for the entire country of Iran is presented in Figure 7.

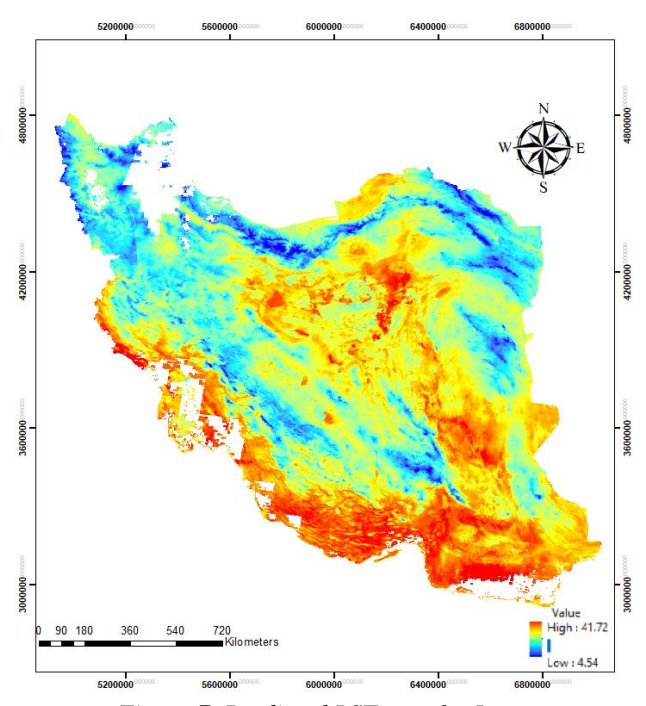


Figure 7. Predicted LST map for Iran

5.2. Cloud Coverage Detection and Creation of Virtual Cloud

Mask

Since it was not possible to validate the model using cloud-covered areas, a virtual cloud mask was created for a sunny day to evaluate the results of the proposed method. The selected area for creating the virtual cloud is the city of Varamin. The black and white cloud mask created is shown in Figure 8, where cloud-covered cells are shown in white and clear sky pixels are shown in black.



Figure 8. Binary cloud mask used for evaluation purposes, created using the administrative boundary of Varamin city. White areas represent simulated cloud-covered pixels, while black areas indicate clear-sky pixels. This mask was applied to simulate missing LST data in a controlled environment.

Virtual Cloud Mask and Evaluation Strategy:

Since accurate ground truth data are not typically available under actual cloud-covered conditions, a virtual cloud mask was generated to enable quantitative model validation. For this purpose, the administrative boundary of Varamin city was used as the masked region. All pixels within this boundary were labelled as "cloud-covered", and the surrounding pixels were treated as clear-sky reference data.

Although this mask does not replicate the spatial and spectral complexity of natural cloud formations, it provides a controlled and consistent framework for evaluating the accuracy of LST reconstruction.

This approach allowed us to objectively compare the reconstructed LST values against known true values within the masked region. While the mask does not mimic the physical behaviour of actual cloud cover, it allows for consistent and reproducible evaluation of model performance in the presence of artificially induced data gaps. Therefore, the conclusions drawn from this validation setup should be interpreted as indicative of the model's potential rather than a definitive assessment under real cloud dynamics.

5.3. Scenario 1: IDW Interpolation and RF Adjustment

IN Scenario 1, a neighborhood window was defined around the cloud-covered region to support spatial interpolation from adjacent cloud-free pixels. The defined one-pixel-wide neighborhood is shown in Figure 9. To optimize performance, two sensitivity analyses were conducted. First, various neighborhood window sizes (ranging from 1 to 11 pixels) were tested to evaluate their effect on interpolation accuracy. Second, the number of

decision trees in the RF model was varied to identify the optimal setting for regression accuracy. As illustrated in Figure 10a, the minimum RMSE was achieved using 9 trees in the RF model. Figure 10b shows that the lowest RMSE occurred when using a one-pixel-wide neighborhood, confirming its suitability for fine-scale spatial estimation. These parameter settings were therefore adopted for the final implementation of Scenario 1.



Figure 9. A binary mask illustrating the defined neighborhood (one-pixel-wide strip around the cloudy area) for Scenario 1, applied in the IDW interpolation process for cloud-covered pixels

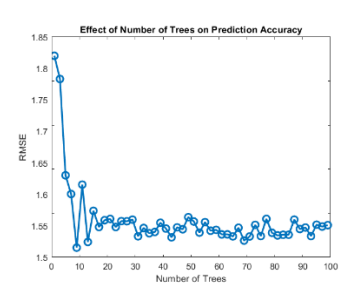


Figure 10a. RMSE values for different numbers of trees in the RF model for Scenario 1. The minimum RMSE was achieved with 9 trees.

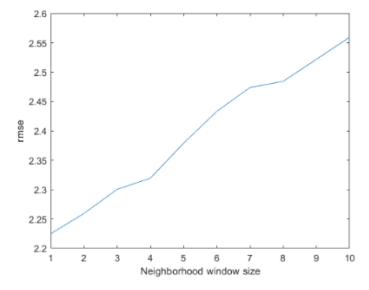


Figure 10b. Relationship between neighborhood window size and interpolation accuracy (RMSE) in Scenario 1. The one-pixel window yielded the highest accuracy.

The sensitivity analyses demonstrate that the interpolation accuracy improves when optimal RF configuration and spatial context are selected. A one-pixel neighborhood provided the highest local relevance for IDW, while a 9-tree RF effectively modeled the relationship between interpolated and actual values.

The accuracy of the initial IDW interpolation and the refined values from the RF model was compared using standard evaluation metrics (RMSE, R, and R²). The results, summarized in **Table 3**, confirm that the improved IDW method significantly enhanced estimation accuracy, reducing RMSE by approximately **0.8°C**.

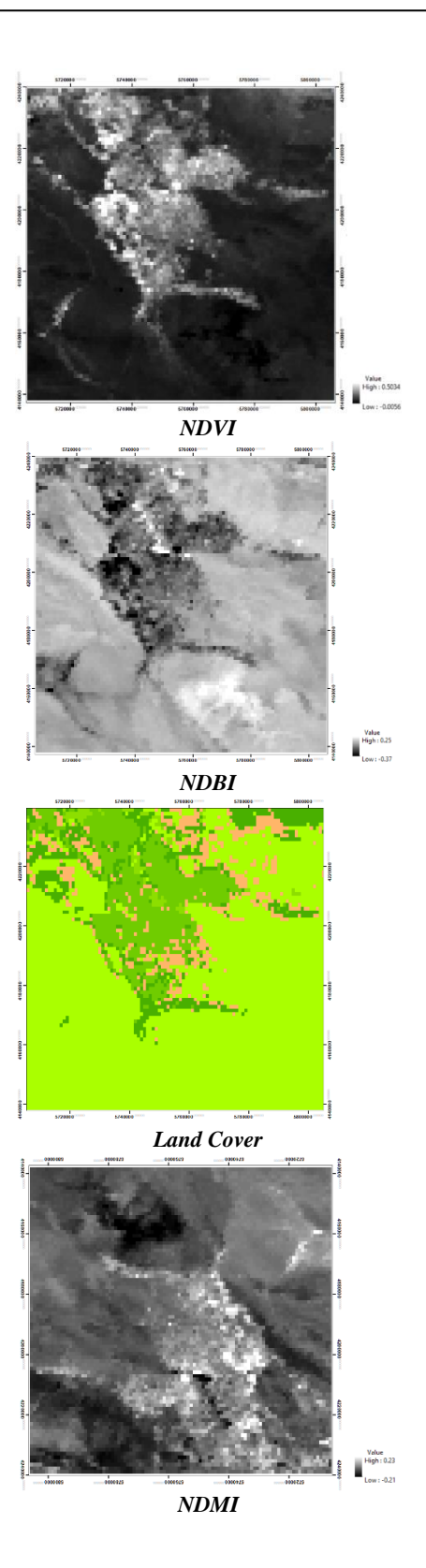
Table 3. Comparison of initial and improved IDW interpolation accuracy using RMSE, R, and R² metrics

	$RMSE(C^{\bullet})$	R	R^2
IDW	2.33	0.72	0.52
Improved IDW	1.53	0.82	0.67

5.4. Scenario 2: Vegetation and Land Cover-Based

Reconstruction

Index Calculation: For Scenario 2, various indices including NDVI, NDBI, NDMI, NDWI, and a land cover classification map—were obtained from MODIS products for the last cloud-free day preceding the study date. These indices were selected due to their known relevance to surface thermal behavior and their ability to capture spatial variations in vegetation, surface moisture, built-up areas, water bodies, and land use types. Specifically, NDVI and NDMI reflect vegetation health and moisture content, NDBI captures built-up surfaces, NDWI identifies water-related features, and land cover categorizes surface types. These features were used as predictors in the Random Forest model to estimate land surface temperatures in cloudcovered regions. The calculated indices are presented in Figure 11, which illustrates their spatial distribution across Tehran Province. These spatial distributions illustrate the variability in land surface characteristics across the study area. As the indices shown in Figure 11 were used as predictors in the Random Forest model for Scenario 2, their spatial heterogeneity directly contributed to improving the accuracy of under-cloud LST reconstruction. The effectiveness of using such indices in LST modeling has also been confirmed in previous studies (Xiao et al., 2021; Yang et al., 2017).



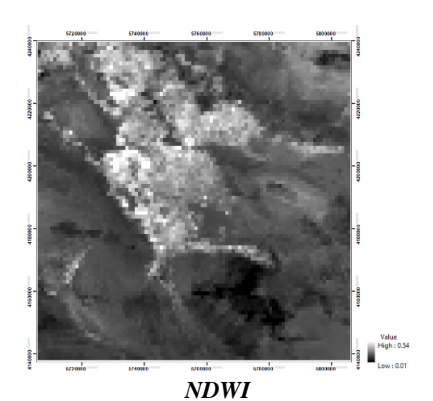


Figure 11. Spatial distribution of the selected indices and land cover over the study area, derived from MODIS data for the most recent cloud-free day prior to the study date

Neighborhood Window Selection: Following the extraction of spectral indices (NDVI, NDBI, NDMI, NDSI) and land cover information for the last cloud-free day (as illustrated in Figure 11), these variables were used as predictors to estimate LST over cloud-covered areas. To optimize model performance, two sensitivity analyses were conducted:

- (1) evaluating the effect of the number of decision trees in the RF model, and
- (2) determining the optimal neighborhood window size to define the spatial training context.

As shown in Figure 13a, the minimum RMSE was obtained with 45 trees in the RF model. Similarly, Figure 13b presents the RMSE trend with different neighborhood sizes, where the optimal performance was achieved using a 7-pixel-wide neighborhood window.



Figure 12. A binary mask illustrating the defined neighborhood (7-pixel-wide strip around the cloudy area) for Scenario 2

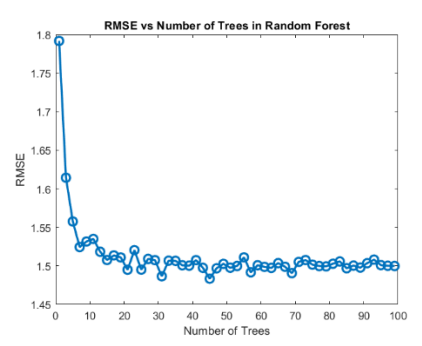


Figure 13a. Sensitivity of RMSE to the number of trees in the RF model for Scenario 2. A minimum RMSE was observed at 45 trees.

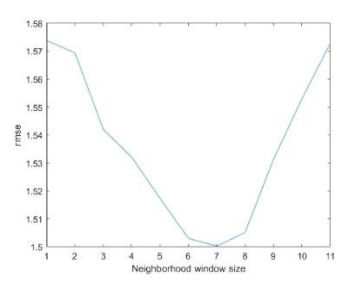


Figure 13b. RMSE as a function of neighborhood window size in Scenario 2. The 7-pixel window provided optimal accuracy.

Accuracy of the RF-Based Method: The accuracy of LST prediction using the RF regression model for Scenario 2 is showed in Table 4. The results show that the RF model effectively reconstructed the LST for cloud-covered regions using the available vegetation and land cover indices.

Table 4. Accuracy metrics (RMSE, R, R²) of the RF model in Scenario 2 for under-cloud LST reconstruction using spectral indicess

	RMSE(C*)	R	R^2
Index Based	1.48	0.78	0.61

5.5. Scenario Combination Using GA

The final step of this study involved combining the outputs of the two scenarios using a GA. This algorithm determined the optimal weights for each scenario based on the RMSE cost function of the LST map. The optimization process of the GA, including the best and mean values, is illustrated in Figure 14. The final LST reconstruction map for the cloud-

covered area is shown alongside the actual LST map in Figure 15.

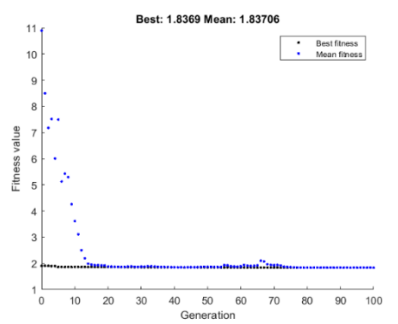


Figure 14. Best and mean values of the GA's optimization process for determining

the weights of the two scenarios.

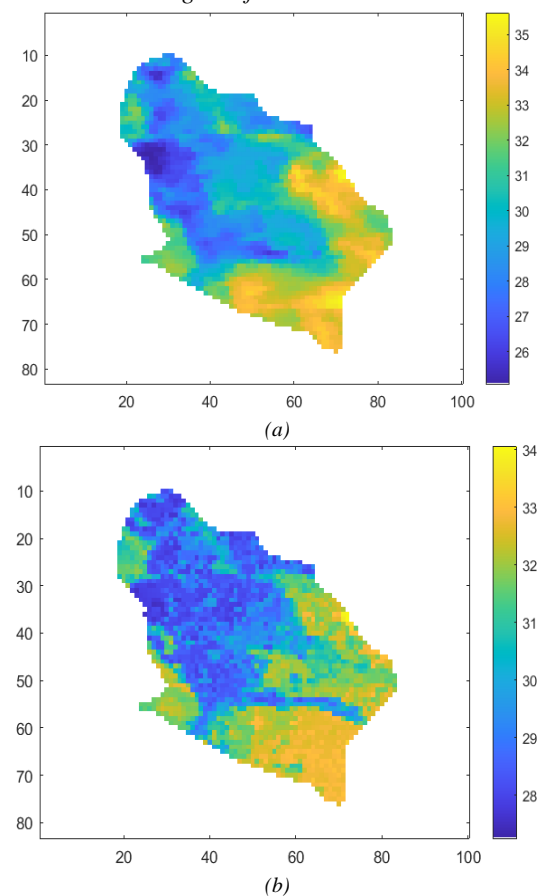


Figure 15. Comparison of (a) the actual LST map obtained from MODIS observations on a cloud-free day, and (b) the predicted LST map generated using the proposed hybrid approach. The prediction was obtained by optimally combining Scenario 1 (interpolation-based) and Scenario 2 (index-based) outputs using a GA. Both maps are displayed in degrees Celsius, with color bars indicating LST values. The reconstructed areas correspond to the simulated cloud-covered region

defined in the virtual mask.

Weighting and Final Results: The weights assigned to each scenario are shown in Table 5. Table 6 compares the accuracy of each individual scenario (1 and 2) with the combined approach using the GA. The results reveal that combining the two scenarios reduced the RMSE by about 0.8°C compared to using each scenario separately, highlighting the improved accuracy of the LST reconstruction when both methods are combined.

Table 5. The weights derived from the GA method for Scenarios 1 and 2

Scenario I	Scenario II	
0.23	0.77	

Table 6. Comparison of the accuracy of Scenarios 1 and 2 and their combination

	$RMSE(C^{\bullet})$	R	R^2
Improved IDW	1.54	0.82	0.67
Index Based	1.48	0.78	0.60
GA-Based Integration	0.79	0.94	0.88

6. Conclusion and Discussion

Applications that analyse satellite images of indices such as LST depend fundamentally on the seasons, i.e., they are limited to carrying out investigations in specific periods due to the presence of cloud cover blocking substantial information that can cause inconsistencies in the analysis.

The aim of this study was to introduce a novel method for reconstructing under-cloud surface temperature using ground station data and combining two different scenarios. for this purpose, in the first scenario, an improved IDW method was used to reconstruct the under-cloud LST. According to what was shown in table 3, the RMSE value of this method was 1.53°C, which showed an improvement of 0.8°C compared to the IDW method. In the second scenario, the index-based method and RF algorithm were used for under-cloud LST reconstruction.

According to Table 4, the RMSE value in this method was 1.48°C. In both scenarios the last cloud - free image and neighborhood pixels on a cloudy day were used for reconstruction.

To optimize performance, in each of the two scenarios,

sensitivity analysis was tested for different window sizes to evaluate their impact on interpolation accuracy (Figures 9 and 12), and the best neighborhood window size were selected. For weighted combination of the results of two scenarios, GA algorithm was used.

The results demonstrated that the use of a GA to combine the two scenarios was effective in improving under-cloud surface temperature reconstruction. By combining the two scenarios, the RMSE of the final LST reconstruction map was reduced by 0.8°C compared to each scenario individually, with the final RMSE of the reconstructed LST map being 0.78°C. Another advantage of the presented method is the conversion of LST obtained from the satellite to near ground LST, for which data from ground stations and the RF method were used, and the results of its evaluation are shown in Table 2.

The comparison of methods revealed that the RF approach, utilizing features such as NDVI and land cover maps, is a powerful tool for reconstructing LST in cloud-covered areas. Furthermore, applying machine learning methods like RF significantly outperformed traditional interpolation techniques. The method presented in this study can be applied to future research in regions experiencing cloud cover challenges.

Limitations and Future Work

As a limitation, comparing the proposed method with deep learning methods was not possible due to the unavailability of sufficient training data and relevant codes. Another limitation of this study is that the performance evaluation was primarily conducted in a relatively flat region (Varamin). As topographic complexity can influence both the accuracy of interpolation techniques and the behaviour of spectral indices used in LST modelling, further validation is necessary in mountainous and topographically diverse regions. Future work should include case studies from such environments to assess the generalizability and robustness of the proposed hybrid approach under varying terrain conditions.

The next limitation lies in the method's reliance on ground station data for calibration and evaluation. In regions where such data are sparse or unavailable, the effectiveness of the model may be reduced. In addition, when cloud cover is very dense or widespread, some remote sensing indices may not be available for a significant portion of the image, leading to decreased reconstruction accuracy.

To address these issues, future studies should explore strategies that reduce dependence on in-situ observations, such as integrating multi-source satellite data (e.g., combining MODIS with Landsat or Sentinel imagery), or developing generalized models that can be applied across various land cover and climatic zones. These enhancements would help improve the flexibility and applicability of the method in more challenging environmental conditions.

Furthermore, to enhance the proposed approach, future work could investigate refined strategies for selecting neighborhood window sizes based on local spatial characteristics. The inclusion of additional predictive features, such as surface albedo or land surface emissivity, may also improve model performance. Applying this method in regions with a denser network of ground meteorological stations could facilitate more detailed validation and potentially increase the accuracy of under-cloud LST reconstruction.

Competing Interests: The authors declare no competing interests.

References

Breiman, L. (2001). Random Forests. Machine Learning, 45(1), 5–32. https://doi.org/10.1023/A:1010933404324 Cho, D., Bae, D., Yoo, C., Im, J., Lee, Y., & Lee, S. (2022). All-Sky 1 km MODIS Land Surface Temperature Reconstruction Considering Cloud Effects Based on Machine Learning. Remote Sensing, 14(8), Article 8. https://doi.org/10.3390/rs14081815

Crosson, W. L., Al-Hamdan, M. Z., Hemmings, S. N. J., & Wade, G. M. (2012). A daily merged MODIS Aqua—Terra land surface temperature data set for the conterminous United States. Remote Sensing of Environment, 119, 315—324. https://doi.org/10.1016/j.rse.2011.12.019

Fan, X.-M., Liu, H.-G., Liu, G.-H., & Li, S.-B. (2014). Reconstruction of MODIS land-surface temperature in a flat terrain and fragmented landscape. International Journal of Remote Sensing, 35(23), 7857–7877. https://doi.org/10.1080/01431161.2014.978036

Freitas, S. C., Trigo, I. F., Macedo, J., Barroso, C., Silva, R., & Perdigão, R. (2013). Land surface temperature from multiple geostationary satellites. International Journal of Remote Sensing, 34(9–10), 3051–3068. https://doi.org/10.1080/01431161.2012.716925

Fu, P., Xie, Y., Weng, Q., Myint, S., Meacham-Hensold, K., & Bernacchi, C. (2019). A physical model-based method for retrieving urban land surface temperatures under cloudy conditions. Remote Sensing of Environment, 230, 111191. https://doi.org/10.1016/j.rse.2019.05.010

Gillespie, A., Rokugawa, S., Matsunaga, T., Cothern, J. S., Hook, S., & Kahle, A. B. (1998). A temperature and

emissivity separation algorithm for Advanced Spaceborne Thermal Emission and Reflection Radiometer (ASTER) images. IEEE Transactions on Geoscience and Remote Sensing, 36(4), 1113–1126. IEEE Transactions on Geoscience and Remote Sensing. https://doi.org/10.1109/36.700995

Gong, Y., Li, H., Shen, H., Meng, C., & Wu, P. (2023). Cloud-covered MODIS LST reconstruction by combining assimilation data and remote sensing data through a nonlocality-reinforced network. International Journal of Applied Earth Observation and Geoinformation, 117, 103195. https://doi.org/10.1016/j.jag.2023.103195

Huang, B., Wang, J., Song, H., Fu, D., & Wong, K. (2013). Generating High Spatiotemporal Resolution Land Surface Temperature for Urban Heat Island Monitoring. IEEE Geoscience and Remote Sensing Letters, 10(5), 1011–1015. IEEE Geoscience and Remote Sensing Letters. https://doi.org/10.1109/LGRS.2012.2227930

Jiménez-Muñoz, J. C., & Sobrino, J. A. (2003). A generalized single-channel method for retrieving land surface temperature from remote sensing data. Journal of Geophysical Research: Atmospheres, 108(D22). https://doi.org/10.1029/2003JD003480

Jiménez-Muñoz, J. C., Sobrino, J. A., Skoković, D., Mattar, C., & Cristóbal, J. (2014). Land Surface Temperature Retrieval Methods From Landsat-8 Thermal Infrared Sensor Data. IEEE Geoscience and Remote Sensing Letters, 11(10), 1840–1843. IEEE Geoscience and Remote Sensing Letters. https://doi.org/10.1109/LGRS.2014.2312032

Jin, M., & Dickinson, R. E. (1999). Interpolation of surface radiative temperature measured from polar orbiting satellites to a diurnal cycle: 1. Without clouds. Journal of Geophysical Research: Atmospheres, 104(D2), 2105–2116. https://doi.org/10.1029/1998JD200005

Kustura, K., Conti, D., Sammer, M., & Riffler, M. (2025). Harnessing Multi-Source Data and Deep Learning for High-Resolution Land Surface Temperature Gap-Filling Supporting Climate Change Adaptation Activities. Remote Sensing, 17(2), Article 2. https://doi.org/10.3390/rs17020318

Liu, H., & Weng, Q. (2009). An examination of the effect of landscape pattern, land surface temperature, and socioeconomic conditions on WNV dissemination in Chicago. Environmental Monitoring and Assessment, 159(1), 143–161. https://doi.org/10.1007/s10661-008-0618-6

Lu, G. Y., & Wong, D. W. (2008). An adaptive inversedistance weighting spatial interpolation technique. Computers & Geosciences, 34(9), 1044–1055. https://doi.org/10.1016/j.cageo.2007.07.010

Lu, L., Venus, V., Skidmore, A., Wang, T., & Luo, G. (2011). Estimating land-surface temperature under clouds using

MSG/SEVIRI observations. International Journal of Applied Earth Observation and Geoinformation, 13(2), 265–276. https://doi.org/10.1016/j.jag.2010.12.007

Mallick, J., Rahman, A., & Singh, C. K. (2013). Modeling urban heat islands in heterogeneous land surface and its correlation with impervious surface area by using night-time ASTER satellite data in highly urbanizing city, Delhi-India. Advances in Space Research, 52(4), 639–655. https://doi.org/10.1016/j.asr.2013.04.025

Mo, Y., Xu, Y., Chen, H., & Zhu, S. (2021). A Review of Reconstructing Remotely Sensed Land Surface Temperature under Cloudy Conditions. Remote Sensing, 13(14), Article 14. https://doi.org/10.3390/rs13142838

Na, F., Gaodi, X., Wenhua, L., Yajing, Z., Changshun, Z., & Na, L. (2014). Mapping Air Temperature in the Lancang River Basin Using the Reconstructed MODIS LST Data. Journal of Resources and Ecology, 5(3), 253–262. https://doi.org/10.5814/j.issn.1674-764X.2014.03.008

Neteler, M. (2010). Estimating Daily Land Surface Temperatures in Mountainous Environments by Reconstructed MODIS LST Data. Remote Sensing, 2(1), Article 1. https://doi.org/10.3390/rs1020333

Rozenstein, O., Qin, Z., Derimian, Y., & Karnieli, A. (2014). Derivation of Land Surface Temperature for Landsat-8 TIRS Using a Split Window Algorithm. Sensors, 14(4), Article 4. https://doi.org/10.3390/s140405768

Scharlemann, J. P. W., Benz, D., Hay, S. I., Purse, B. V., Tatem, A. J., Wint, G. R. W., & Rogers, D. J. (2008). Global Data for Ecology and Epidemiology: A Novel Algorithm for Temporal Fourier Processing MODIS Data. PLOS ONE, 3(1), e1408. https://doi.org/10.1371/journal.pone.0001408 Ullah, M., Li, J., & Wadood, B. (2020). Analysis of Urban Expansion and its Impacts on Land Surface Temperature and Vegetation Using RS and GIS, A Case Study in Xi'an City, China. Earth Systems and Environment, 4(3), 583–597. https://doi.org/10.1007/s41748-020-00166-6

Wan, Z. (2008). New refinements and validation of the MODIS Land-Surface Temperature/Emissivity products. Remote Sensing of Environment, 112(1), 59–74. https://doi.org/10.1016/j.rse.2006.06.026

Wan, Z., & Dozier, J. (1996). A generalized split-window algorithm for retrieving land-surface temperature from space. IEEE Transactions on Geoscience and Remote Sensing, 34(4), 892–905. IEEE Transactions on Geoscience and Remote Sensing. https://doi.org/10.1109/36.508406

Wang, Q., Tang, Y., Tong, X., & Atkinson, P. M. (2024). Filling gaps in cloudy Landsat LST product by spatial-temporal fusion of multi-scale data. Remote Sensing of Environment, 306, 114142.

https://doi.org/10.1016/j.rse.2024.114142

Wu, P., Su, Y., Duan, S., Li, X., Yang, H., Zeng, C., Ma, X., Wu, Y., & Shen, H. (2022). A two-step deep learning

framework for mapping gapless all-weather land surface temperature using thermal infrared and passive microwave data. Remote Sensing of Environment, 277, 113070. https://doi.org/10.1016/j.rse.2022.113070

Xiao, Y., Zhao, W., Ma, M., & He, K. (2021). Gap-Free LST Generation for MODIS/Terra LST Product Using a Random Forest-Based Reconstruction Method. Remote Sensing, 13(14), Article 14. https://doi.org/10.3390/rs13142828 Xu, Y., & Shen, Y. (2013). Reconstruction of the land surface temperature time series using harmonic analysis.

temperature time series using harmonic analysis.

Computers & Geosciences, 61, 126–132.

https://doi.org/10.1016/j.cageo.2013.08.009

Yang, Y., Cao, C., Pan, X., Li, X., & Zhu, X. (2017). Downscaling Land Surface Temperature in an Arid Area by Using Multiple Remote Sensing Indices with Random Forest Regression. Remote Sensing, 9(8), Article 8. https://doi.org/10.3390/rs9080789

Yu, W., Nan, Z., Wang, Z., Chen, H., Wu, T., & Zhao, L. (2015). An Effective Interpolation Method for MODIS Land Surface Temperature on the Qinghai—Tibet Plateau. IEEE Journal of Selected Topics in Applied Earth Observations and Remote Sensing, 8(9), 4539–4550. IEEE Journal of

Selected Topics in Applied Earth Observations and Remote Sensing. https://doi.org/10.1109/JSTARS.2015.2464094

Yu, X., Guo, X., & Wu, Z. (2014). Land Surface Temperature Retrieval from Landsat 8 TIRS—Comparison between Radiative Transfer Equation-Based Method, Split Window Algorithm and Single Channel Method. Remote Sensing, 6(10), Article 10. https://doi.org/10.3390/rs6109829

Zhao, B., Mao, K., Cai, Y., Shi, J., Li, Z., Qin, Z., Meng, X., Shen, X., & Guo, Z. (2020). A combined Terra and Aqua MODIS land surface temperature and meteorological station data product for China from 2003 to 2017. Earth System Science Data, 12(4), 2555–2577. https://doi.org/10.5194/essd-12-2555-2020

Zhou, J., Liang, S., Cheng, J., Wang, Y., & Ma, J. (2019). The GLASS Land Surface Temperature Product. IEEE Journal of Selected Topics in Applied Earth Observations and Remote Sensing, 12(2), 493–507. IEEE Journal of Selected Topics in Applied Earth Observations and Remote Sensing. https://doi.org/10.1109/JSTARS.2018.2870130